

EGU General Assembly 2020

Mantle flow under the Central Alps: Constraints from non-vertical-ray SKS shear-wave splitting

- 04.05.2020 -

Eric Löberich¹ and Götz Bokelmann¹

¹ Department of Meteorology and Geophysics, University of Vienna, Vienna, Austria



Outline

- 1. Introduction 3 - 5
- 2. Method 6 - 8
- 3. Data 9 - 10
- 4. Results & Discussion 11 - 15
- 5. Conclusion 16
- 6. References 17





1. Introduction

1.1 Seismic anisotropy

➤ Definition (Mainprice, 2015)

“Seismic anisotropy is commonly defined as the direction-dependent nature of the propagation velocities of seismic waves. [...] In addition [...] there is direction-dependent polarization of P- and S-waves, and anisotropy can contribute to the splitting of normal modes.”

➤ Lattice-preferred orientation (LPO) (Becker, 2011)

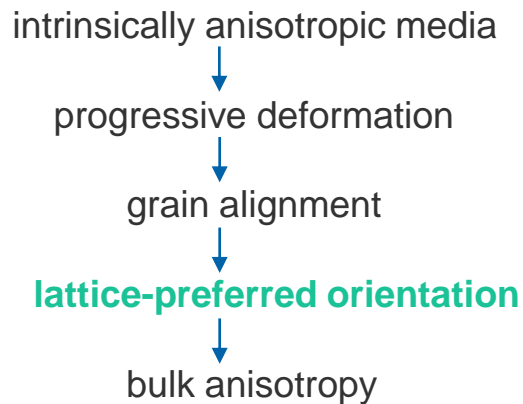


Fig. 1 Olivine (Weinrich, 2016)

➤ LPO anisotropy in the upper mantle (Mainprice, 2015; Babuska and Cara, 1991)

- > olivine (orthorhombic)
- > orthopyroxene (orthorhombic)
- > clinopyroxene (monoclinic)
- > garnet (cubic)





1. Introduction

1.2 Shear-wave splitting and SK(K)S-phase (Becker, 2011, references therein)

➤ Shear-wave splitting (SWS)

- > seismic anisotropy detection:
 - body-wave method
 - incoming S-wave effected by azimuthal anisotropy
 - fast/slow polarization direction
 - similar to optical birefringence
- separation of two quasi-shear waves
- > splitting parameters:
 - φ ... fast orientation (horizontal)
 - Δt ... delay time (fast - slow arrival)
- > resolution:
 - laterally good (~ 50km)
 - worse in depth

➤ SK(K)S-phase

- > core phases:
 - S-P-S conversion
 - removed source-side anisotropy
- > hypocentral distance $90^\circ - 130^\circ$:
 - vertical incidence approximation
- > **Is this a suitable simplification or do we lose useful information?**

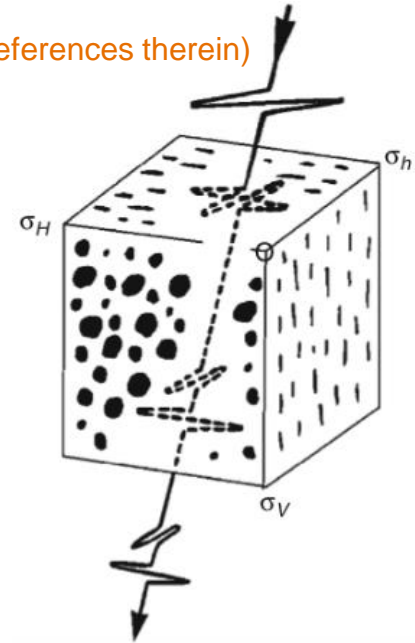


Fig. 2 SWS scheme (Crampin, 2011)

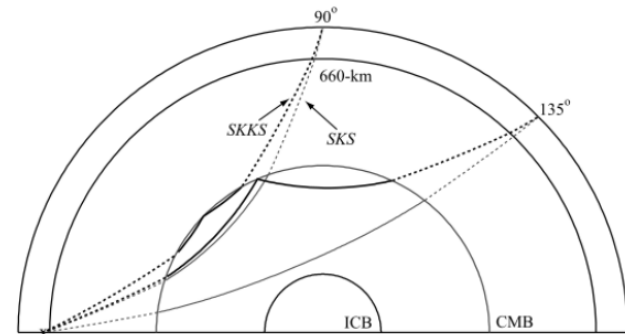


Fig. 3 SKS and SKKS ray path (Niu and Perez, 2004)





1. Introduction

1.3 Geodynamic models (Silver, 1996)

➤ Simple asthenospheric flow (SAF)

- > relative motion between lithosphere & mantle below asthenosphere:
 - strain accumulation in asthenosphere
 - horizontal foliation & lineation following flow line
 - a-axis & $\phi \parallel$ absolute plate motion direction
- > associated with b-up olivine

➤ Vertical coherent deformation (VCD)

- > transpressional or extensional movement:
 - $\phi \parallel$ deformation direction
- > further shear activity (transpress. case):
 - sub-horizontally oriented lineation, a-axis & ϕ in vertically aligned planes of foliation
- > associated with c-up olivine

➤ Can we distinguish both models from SWS measurements?

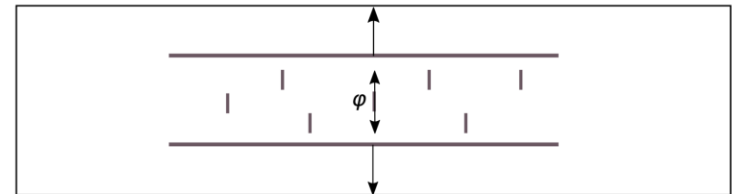
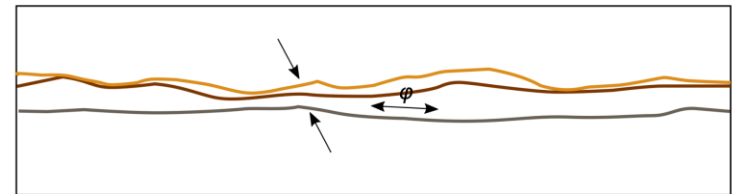
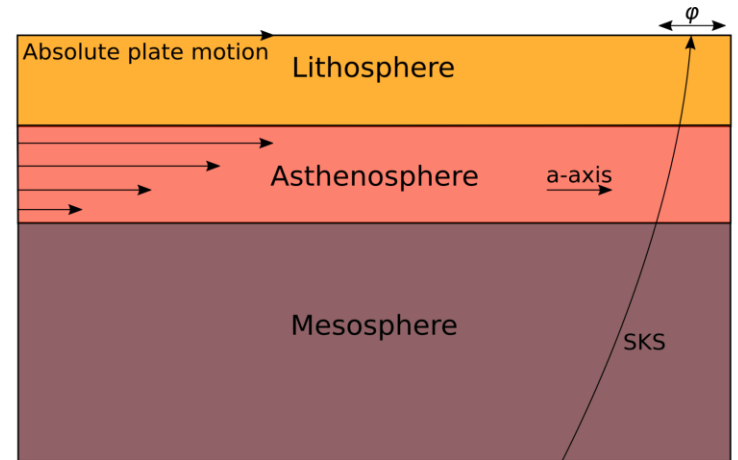


Fig. 4 SAF (top) and VCD (bottom) (based on Silver, 1996)





2. Method

2.1 S-wave propagation in anisotropic media (e.g. Davis, 2003)

➤ Fast orientation approximation for non-vertical incidence

$$\rho v_s^2 = C_{ijkl} v_j v_k s_i s_l \quad (1)$$

$$\phi = \phi_0 + \delta\phi_f \quad (2)$$

$$\phi = \phi_0 + d_1 \sin(2z)\theta^2 \quad (3)$$

$$d_1 = -f_1/f_4 \quad (4)$$

$$C_{ijkl} = \begin{bmatrix} C_{1111} & C_{1122} & C_{1133} & 0 & 0 & 0 \\ C_{1122} & C_{2222} & C_{2233} & 0 & 0 & 0 \\ C_{1133} & C_{2233} & C_{3333} & 0 & 0 & 0 \\ 0 & 0 & 0 & C_{2323} & 0 & 0 \\ 0 & 0 & 0 & 0 & C_{1313} & 0 \\ 0 & 0 & 0 & 0 & 0 & C_{1212} \end{bmatrix}$$

$$f_1 = C_{1212} - C_{2233} - C_{1133} - 2C_{1313} + C_{1122} - C_{2323} + C_{3333} \quad (5)$$

$$f_4 = -2C_{1313} + 2C_{2323} \quad (6)$$

C_{ijkl} ... anisotropic stiffness tensor
(stress-strain relation)

ρ ... density

$[\nu_1, \nu_2, \nu_3]$... travel direction

V ... phase velocity (eigenvalues)

S_i ... polarization of the phase
(eigenvectors)

z ... azimuth

θ ... incidence angle ($< 30^\circ$)





2. Method

2.2 Non-vertical-ray shear-wave splitting approach

➤ Azimuthal variation of SWS parameters

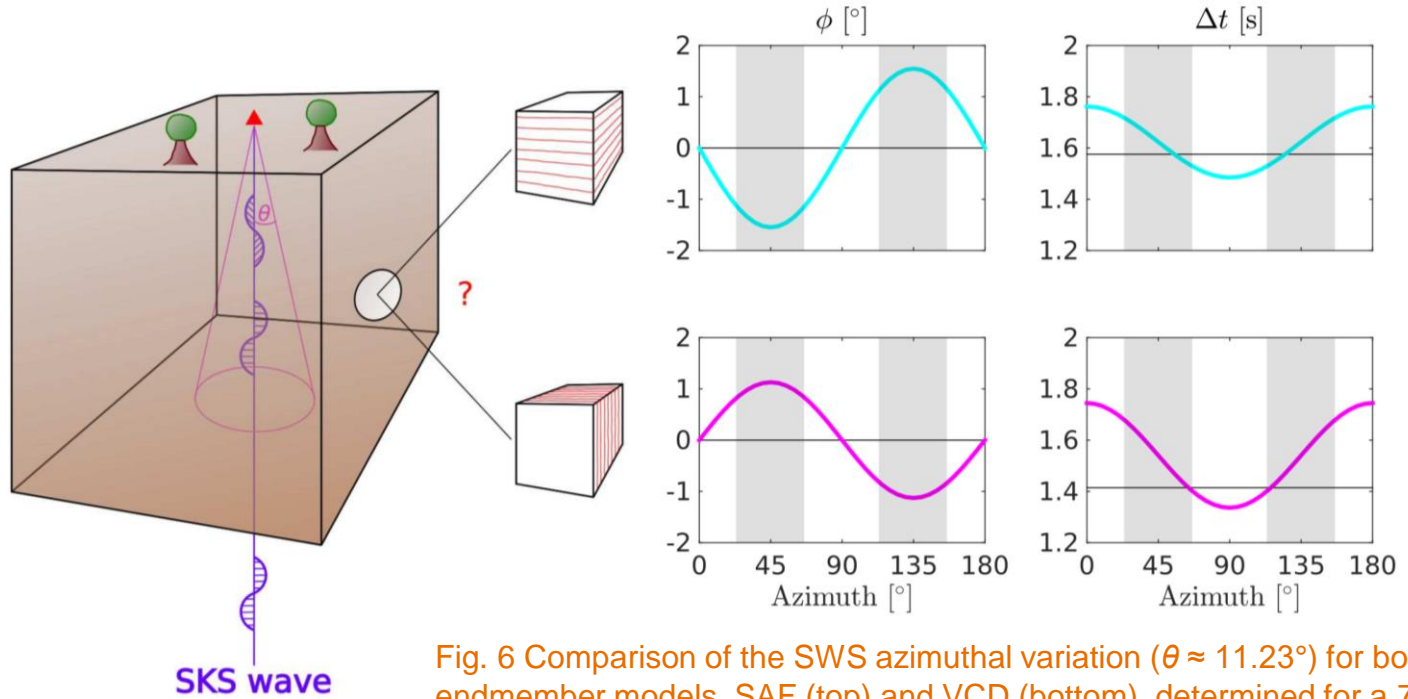


Fig. 6 Comparison of the SWS azimuthal variation ($\theta \approx 11.23^\circ$) for both endmember models, SAF (top) and VCD (bottom), determined for a 70% **b-up** ($d_{1b} \approx -0.7$) or **c-up** ($d_{1c} \approx 0.51$) olivine orientation (layer: 100km). The black line indicates the corresponding vertical incidence case.

- > **b-** and **c-up** olivine SWS backazimuth (Baz) variation differ
- > polarity & amplitude of ϕ controlled by oscillation parameter d_1
- > **SAF & VCD distinguishable by the non-vertical-ray SWS approach**





2. Method

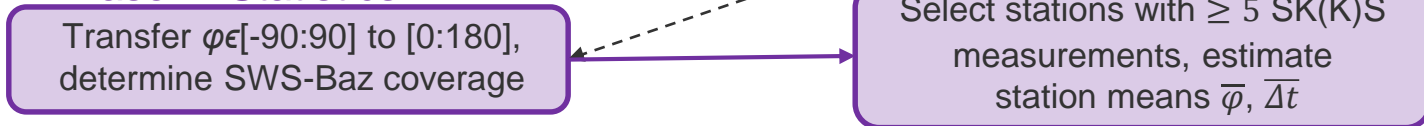
2.2 Non-vertical shear-wave splitting approach

➤ Workflow

-> Phase I: Selection



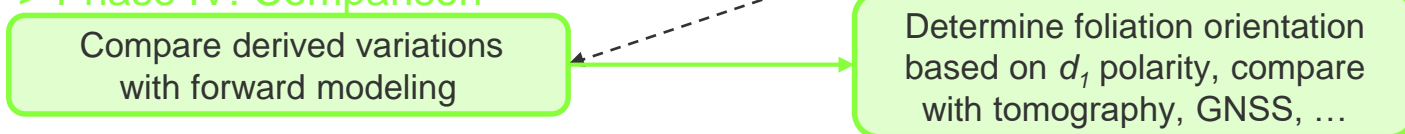
-> Phase II: Statistics



-> Phase III: Correction



-> Phase IV: Comparison

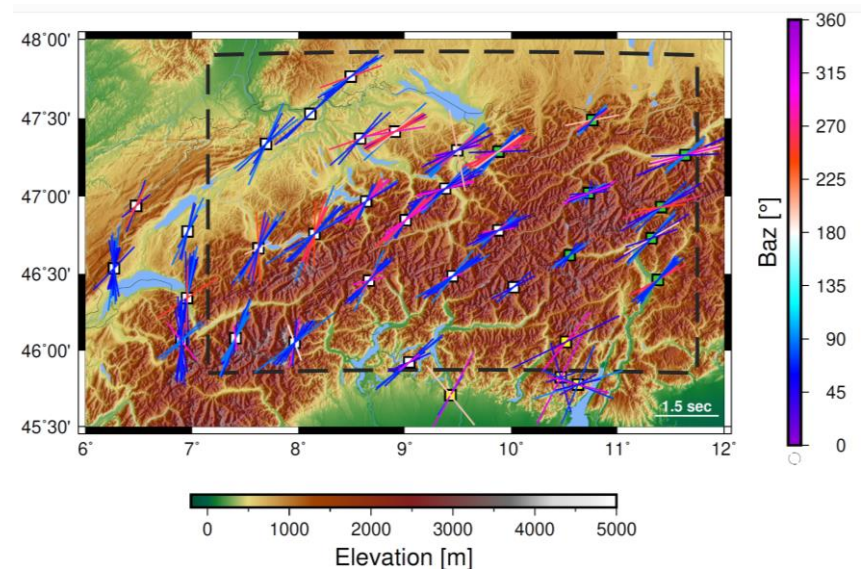
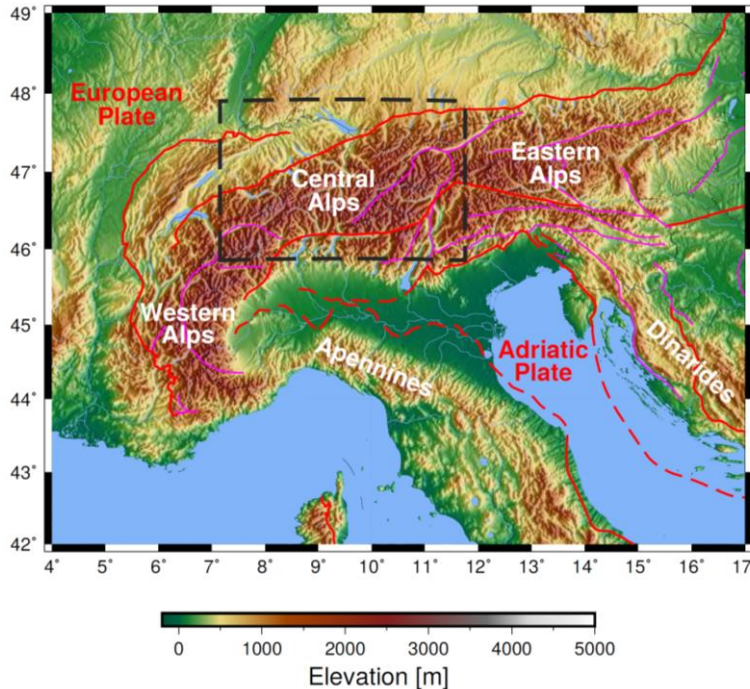




3. Data

3.1 Phase I - Selection

➤ Overview



➤ Individual SWS measurements

- > Barruol et al. (2011): - SDSN/CH (2006-2008)
- Δ : 85° - 120°, $M > 6$
- > Qorbani et al. (2015): - OE (2002-2013)
- Δ : 90° - 130°, $M > 6$
- > Salimbeni et al. (2018): - IV (2012-2013)
- Δ : 80° - 120°, $M > 5.8$
- > phases: SK(K)S
- > SWS: Minimum energy technique
(Silver and Chan, 1991)

Fig. 7 (left) The study region (dashed rectangle) on a topographic map (Amante and Eakins, 2009). Deformation fronts (red solid: exposed, red dashed: sub-surface, magenta: Neogene fault) are taken from the Alpine geological map (4D-MB SPP, 2019, based on Schmid et al., 2004; Schmid et al., 2008). (right) Mountain-chain-parallel pattern of high-quality ($\sigma_\phi \leq 20^\circ$) SWS measurements (permanent stations in white: Barruol et al., 2011; green: Qorbani et al., 2015; yellow: Salimbeni et al., 2018) on a topographic map (based on Ferranti and Hormann, 2014). Line lengths give splitting delay Δt , orientation the fast orientation ϕ .





3. Data

3.2 Phase II - Statistics

➤ Histograms of SWS parameters

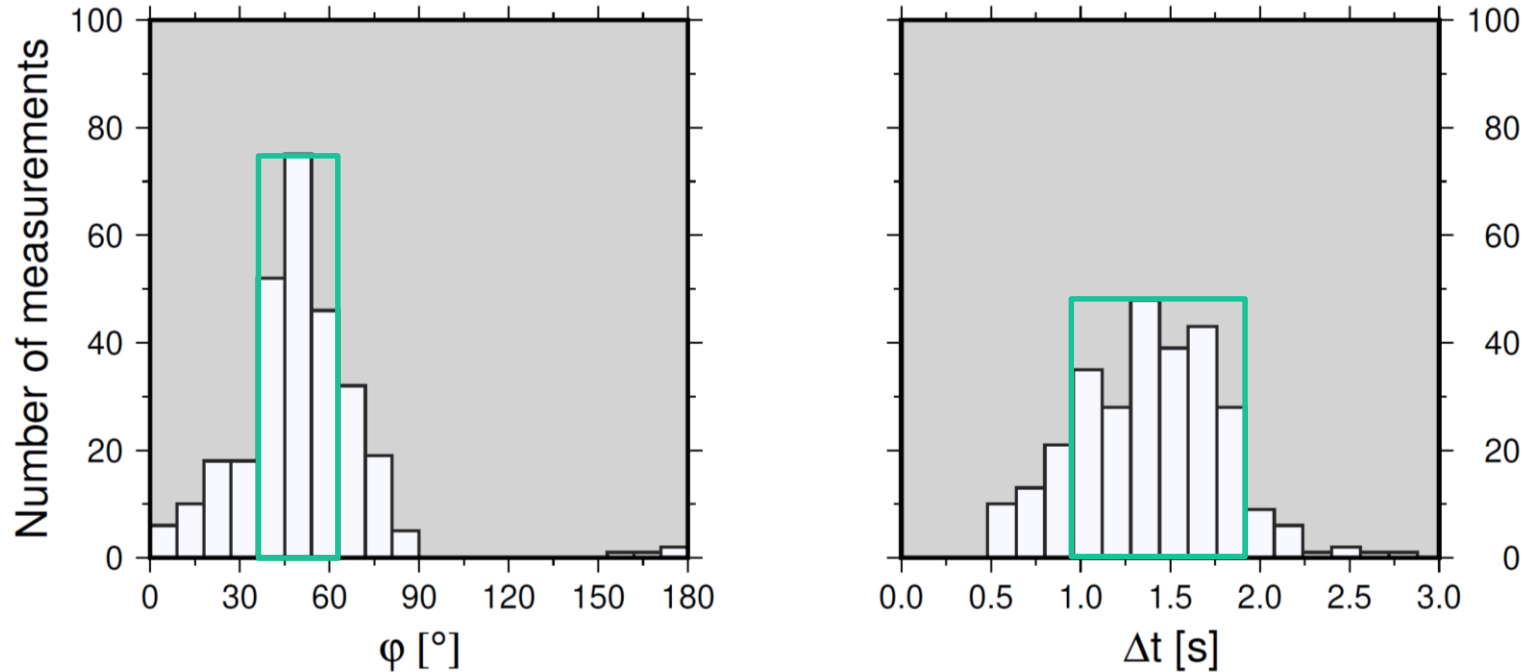


Fig. 8 Statistical distribution of measurements in the study area. Fast orientations (left) indicate a unimodal distribution around **NE-SW** related to the clockwise rotation of ϕ from NNE-SSW in the west to NE-SW in the east (see Fig. 7). Delay times Δt (right) occur in a range between $\sim 0.48 - 2.88$ s, with an accumulation between $\sim 0.96 - 1.92$ s.





4. Results & Discussion

4.1 Phase III & IV - Correction & Comparison

➤ Angular dependence of SWS parameters

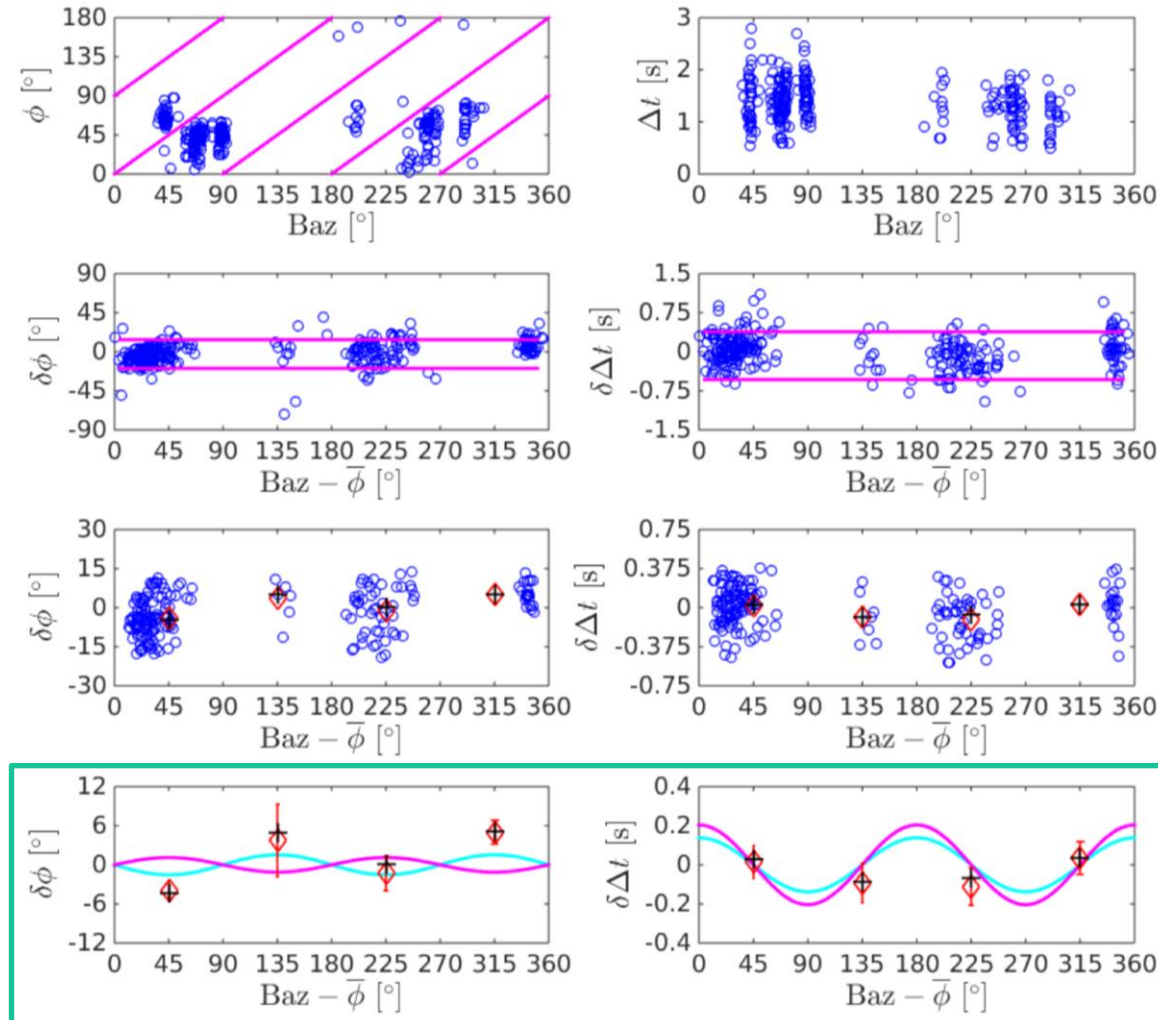


Fig. 9 (top) Baz distribution of ϕ (left, magenta lines: Null direction) and Δt (right) in the Central Alps. (second row) Variations $\delta\phi$ and $\delta\Delta t$ from station averages are shown with thresholds (magenta lines) for the calculation of mean (diamond) and median (plus) inside $\pm 33.25^\circ$ intervals (third row). (bottom) Comparison with expected variations of **b-up** and **c-up** olivine orientation (see Fig. 6).

-> A **b-up olivine situation in the study area and a horizontal flow plane of deformation (SAF model) is likely.**





4. Results & Discussion

4.2 Phase IV - Comparison with Vp anomalies

- P-wave tomography (Koulakov et al., 2009)
 - > **low-velocity**: - hotter, deformable material
 - Western Alps counterflow
 - > **high-velocity**: - colder, lithospheric structures
 - European slab (+ detachment)

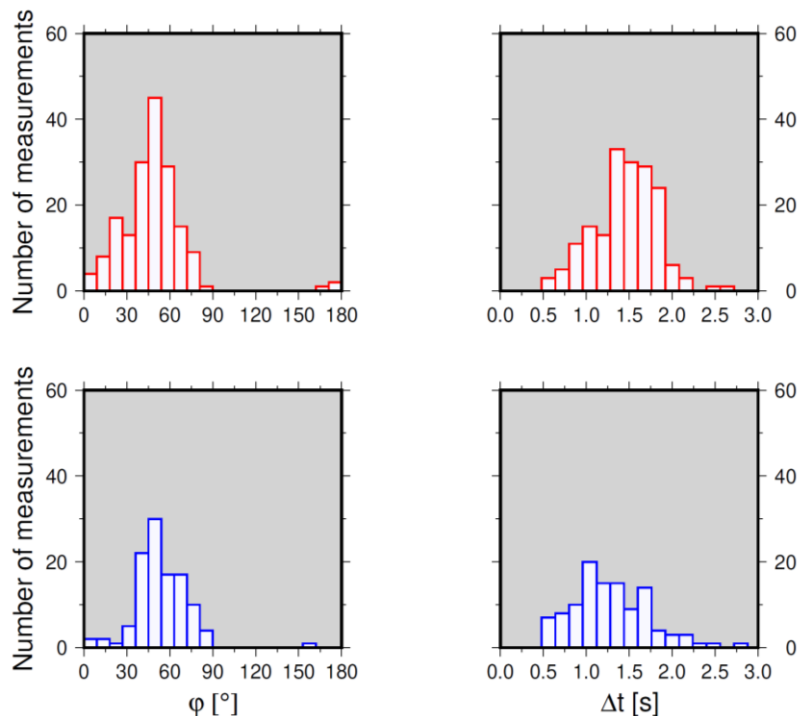


Fig. 11 Histograms of fast orientations φ (left) and delay times Δt (right) per subarea reveal a **larger rotation of φ** and a **tendency to higher Δt** in the **northern** subarea.

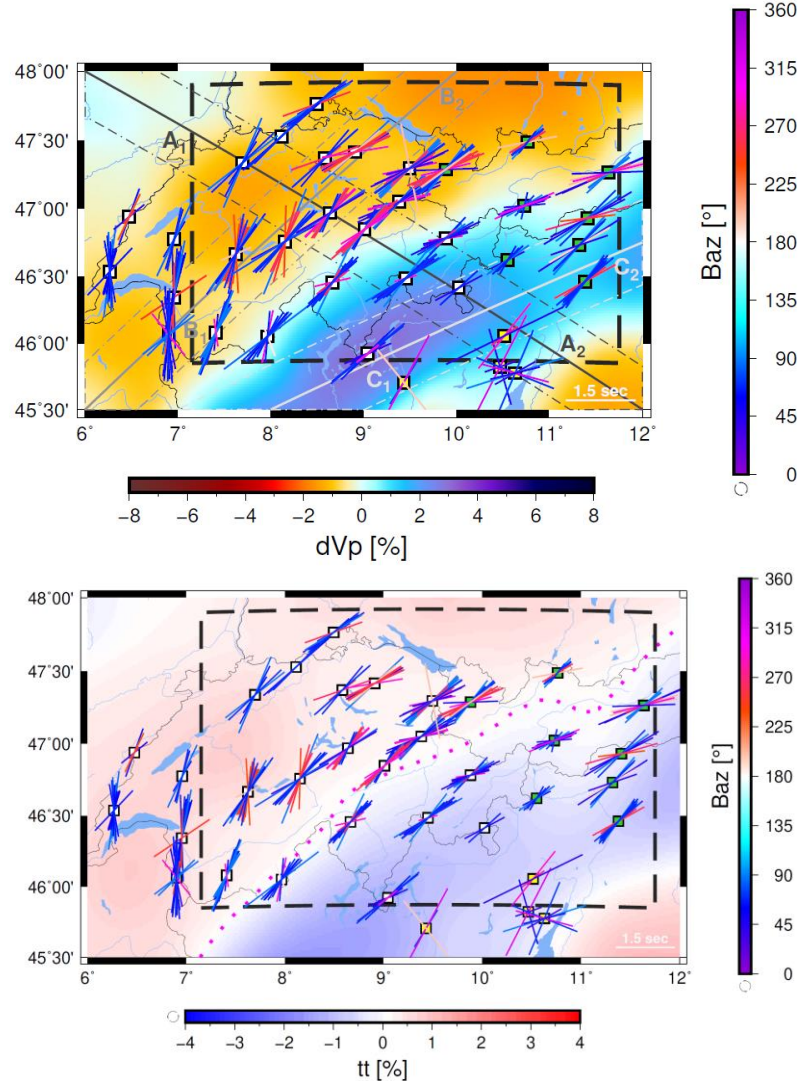


Fig. 10 Comparison of SWS pattern and P-wave velocity perturbations dVp based on Koulakov et al. (2009) in 150km depth (top) and vertically-integrated travel times tt (bottom). Magenta dots separate **northern** and **southern** subarea.





4. Results & Discussion

4.3 Correction & Comparison per subarea

➤ Angular dependence of SWS parameters in subareas

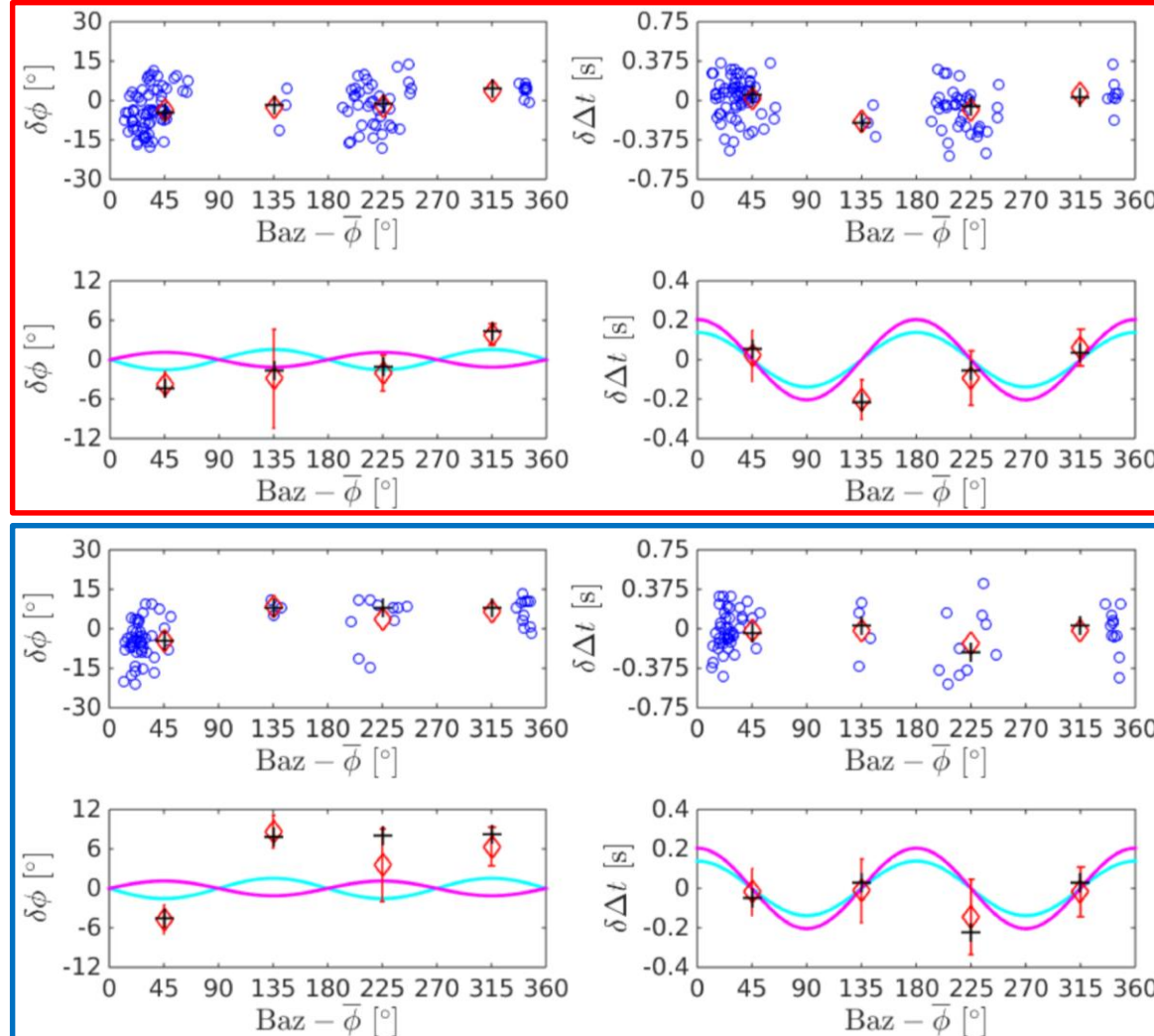


Fig. 12 Comparison of derived angular variations of SWS measurements in the **northern** and **southern** subarea as in Fig. 9 with expected variations of **b-up** and **c-up** olivine orientation (see Fig. 6).

-> $\delta\phi$ and $\delta\Delta t$ behave similar as in the whole study region, an olivine **b-up** orientation / asthenospheric cause is likely

-> Significance of investigated intervals is lower (reduced coverage), both olivine orientations cannot be distinguished with the current amount of high-quality SWS data

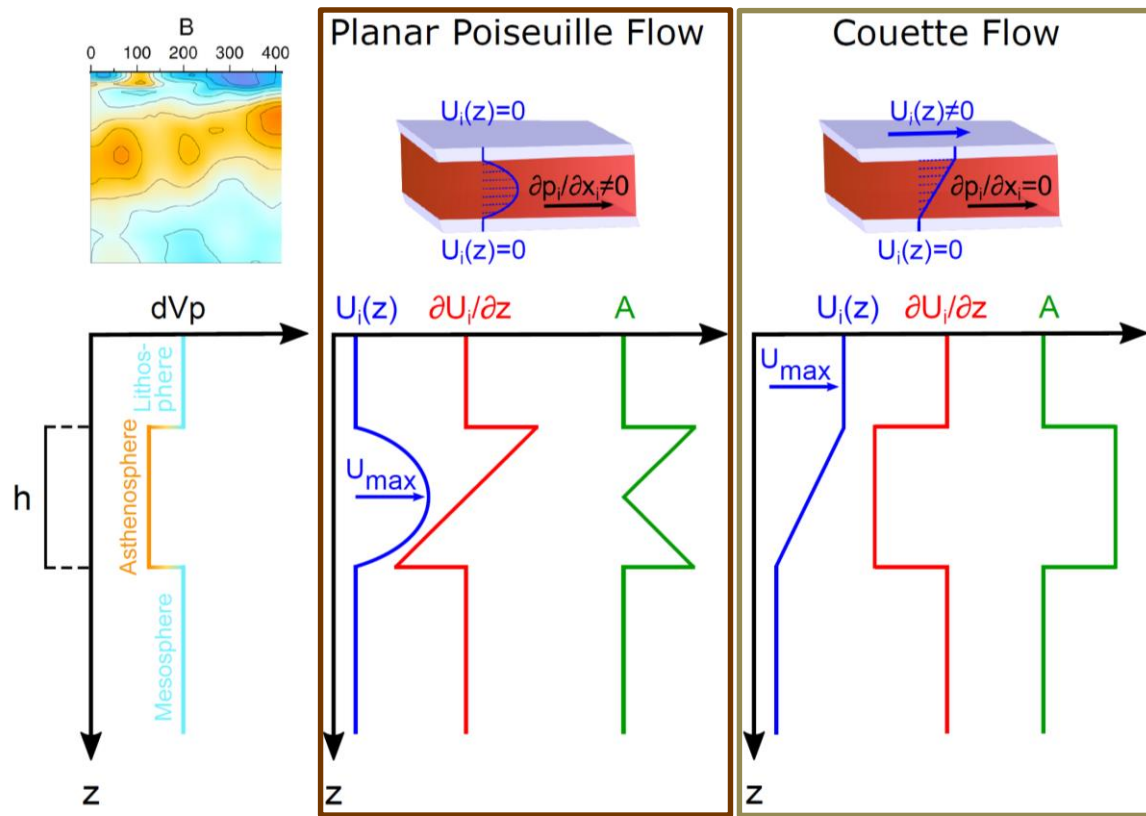




4. Results & Discussion

4.4 Determining the flow type in the northern subarea

➤ Comparing flow types



-> SAF model illustrates Couette flow, expected to control intraplate domains (Natarov and Conrad, 2012, based on Turcotte and Schubert, 2002)

-> Poiseuille flow occurs in areas of changing horizontal pressure, as in the vicinity of subduction zones (Natarov and Conrad, 2012, references therein)

Fig. 12 The two deformation models considered for the upper mantle; (left) Seismic low-velocity zone indicating the deforming zone (see Fig. 10), (center) **planar Poiseuille flow (channel flow)**, and (right) **Couette flow**. Blue colors indicate flow velocity, red colors the vertical gradient of flow, and green the related deformation (based on Brennen, 2006; Richardson, 2011a, 2011b), and anisotropy (Barruol et al., 2019).





4. Results & Discussion

4.4 Determining the flow type in the **northern** subarea

- Can a pure Couette Flow (SAF) explain the ϕ pattern?
 - > no, crustal motions (GNSS) and upper mantle movement reveal opposite sense of rotation
 - > surface motion implies sinistral sense of rotation with progressively larger northward motion toward east
 - > **flow decoupled from lithospheric movement (Barruol et al., 2019)**

- Poiseuille flow
 - > the more likely deformation model, consistent with the vertical alignment of olivine b-axes found in our study
 - > **pulling force of Apenninic slab roll-back leads to changes in pressure field**

- Plane Couette-Poiseuille flow (Natarov and Conrad, 2012, references therein)
 - > **Couette and Poiseuille flow can occur simultaneously,**
 - > 40% of the flow at global scale occurs as Poiseuille flow (similar for Central Europe)
 - > together they produce a changing orientation of shear, if pressure in an orthogonal direction to the plate movement is not constant

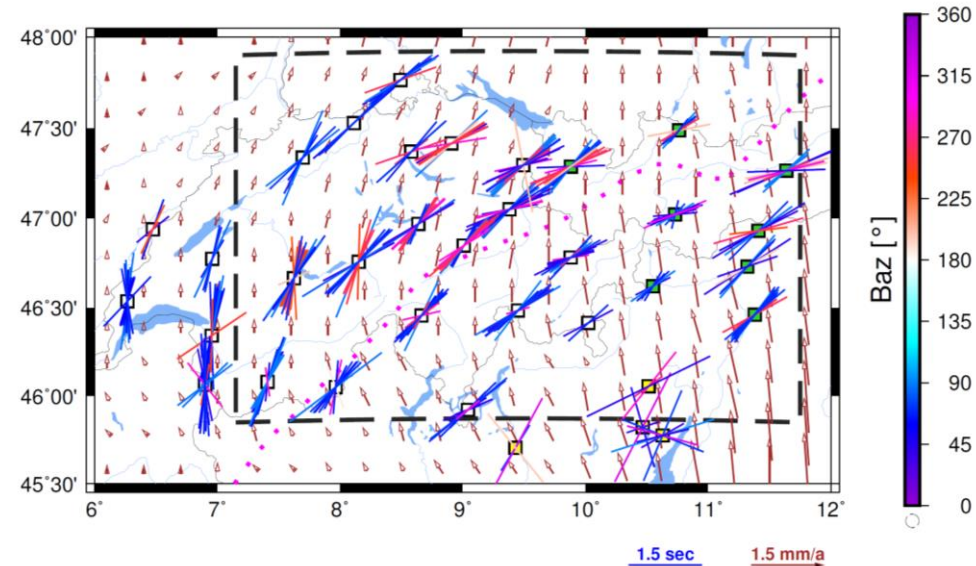


Fig. 13 Comparison of SWS measurements with surface motions (brown arrows) interpolated from GNSS data by Sánchez et al. (2018). The crustal motion pattern generally differs from the fast orientations ϕ . A tendency to small, NNE oriented motions in the **northern** subarea and slightly stronger, NNW oriented motions in the **southern** subarea is revealed.



5. Conclusion

➤ Motivation

- > **constrain subsurface deformation** using Baz variations of SK(K)S splitting data
- > different foliation orientation -> **φ -Baz phase shift**, different φ and Δt amplitudes
- > phase shift of φ -Baz due to polarity of oscillation parameter d_1 related to stiffness tensor:

VCD -> vertical foliation in lithosphere -> **c-up olivine: $d_1 > 0$**
SAF -> horizontal foliation in asthenosphere -> **b-up olivine: $d_1 < 0$**

➤ General observations for the Central Alps

- > whole study area: - φ || mountain-chain; $\Delta t \sim 0.48 - 2.88s$
 - $\delta\varphi / \delta\Delta t$ -Baz variation -> **b-up orientation -> SAF**
- > **northern** subarea: - φ rotates along the Alps; tend to larger Δt ($\sim 1.28 - 1.92s$)
(low $dV\rho$, slow tt) - $\delta\varphi / \delta\Delta t$ -Baz variation -> **likely b-up orientation**
 - little relation between mantle and current crustal deformation
 - > **pure Couette flow (SAF) unlikely**
 - Apenninic slab rollback causes mass deficit / pressure difference
 - > **Poiseuille flow contribution (plane Couette-Poiseuille flow?)**
- > **southern** subarea: - φ shows little rotation; tend to smaller Δt ($\sim 0.96 - 1.76s$)
(high $dV\rho$, fast tt) - $\delta\varphi$ and $\delta\Delta t$ -Baz variation -> **not explainable by SAF or VCD**
 - **Δt and tt correlation suggest lithospheric contribution**
 - contribution from flow below European slab detachment and serpentinization above slab possible



6. References

For further reading:

Löberich, E. and Bokelmann, G.: Mantle flow under the Central Alps: Constraints from non-vertical SKS shear-wave splitting, *Solid Earth Discuss.*, <https://doi.org/10.5194/se-2020-5>, in review, 2020

